Monte Carlo simulation of a typical ^{60}Co therapy source

G. M. Mora and A. Maio
CFNUL and FCUL, Universidade de Lisboa, Av. Prof. Gama Pinto 2, 1649 Lisboa, Portugal

D. W. O. Rogers[a)]
National Research Council of Canada, Ottawa K1A 0R6, Canada

(Received 19 May 1999; accepted for publication 5 August 1999)

The BEAM Monte Carlo code is used to simulate the ^{60}Co beam from an Eldorado 6 radiotherapy unit and to calculate the relative air-kerma output factors as a function of field size. The unit is realistically modeled, including source capsule, housing and collimator assembly. The calculated relative air-kerma output factors at SSD=80.5 cm agree to within 0.1% with measured values. It is shown that the variation of the output factor is almost entirely due to scattered photons from the fixed and adjustable collimators and there is no effect of shadowing primary photons. The influence of the geometry of the collimation system on the photon spectra on-axis is shown to be small but finite. The calculated buildup region of a depth-dose curve in a water phantom irradiated by a narrow and a broad ^{60}Co beam is shown to agree with experimental data at the 2% to 3% level. Unlike previous calculations, the results accurately predict the effects of electron contamination from the surface to dose maximum. The variation of electron contamination with field size is also presented, as are spectra as a function of field size. © *1999 American Association of Physicists in Medicine.* [S0094-2405(99)01111-6]

I. INTRODUCTION

Although ^{60}Co decays with only two gamma-ray lines at 1.17 and 1.33 MeV, it is well known that the spectrum of photons from an encapsulated source contains many other components. Aitken and Henry[1] made extensive measurements for different forms of capsule and an ICRU report gave a detailed review of the measurements and early Monte Carlo calculations of these units.[2] More recently, there have been sophisticated Monte Carlo simulations of the entire ^{60}Co unit.[3–5] However, one study only investigated broad beam conditions,[3] and, while another did investigate different field sizes,[4] it did not correctly predict the experimentally observed variation in output with field size.[6] Han *et al.*[4] calculated a variation in output of 13% whereas the measured value varied by only 7%. Both these previous works modeled cylindrical symmetry about the beam axis and solid collimators instead of the complex leaves of the collimator structure. Although Shipley and Duane used a more realistic model of their Mobaltron ^{60}Co unit, they had trouble predicting their measured TPRs,[5] although that was likely due to inadequate statistics in the calculation. In the present study we use the BEAM-EGS4 code,[7,8] to simulate the ^{60}Co beam and we simulate a more realistic model of the unit with a high degree of statistical precision. We also simulate the collimation system using a simplified model consisting of solid blocks of lead and compare the results with the more realistic simulation.

The detailed description of the basic components of the therapy unit allows us to calculate their contribution to the energy spectrum of the particles which reach the patient.

A detailed Monte Carlo study of electron contamination of ^{60}Co beams and its effects on the depth-dose curves was done in the past,[3] but that work was restricted to broad beams (35×35 cm^2) and made several approximations required by the much slower computers used. In the present work we calculate the central-axis depth-dose curves in a water phantom using simulated narrow and broad ^{60}Co beams, and compare them with the experimental results.[9] The influence of the electron component on the total build up dose curve is presented for both geometries of the beam.

II. CALCULATIONS

A. Geometry of the "Eldorado 6" ^{60}Co unit

The Eldorado 6 (manufactured by Theratronics) is a typical ^{60}Co therapy unit. It consists of a source capsule which contains radioactive ^{60}Co pellets, an immovable primary collimator, an outer set of movable collimators which define the various field sizes of the therapy beam and an overall shield for radiation protection. We realistically model the unit including source, source housing, primary collimator and adjustable leaf collimator assembly. All air gaps between the components are included in our modeling. Figure 1 shows the model of the Eldorado 6 ^{60}Co as used in this study.

1. The capsule

We model a typical capsule size used by Eldorado units with cylindrical geometry about the beam axis. Figure 2 shows a schematic of the source and housing as modeled in our computer simulation. Although we model the ^{60}Co region as a uniform active material region of cobalt of 2 cm diameter, the actual source is made up of many small pellets. The density is reduced to account for the loose packing and

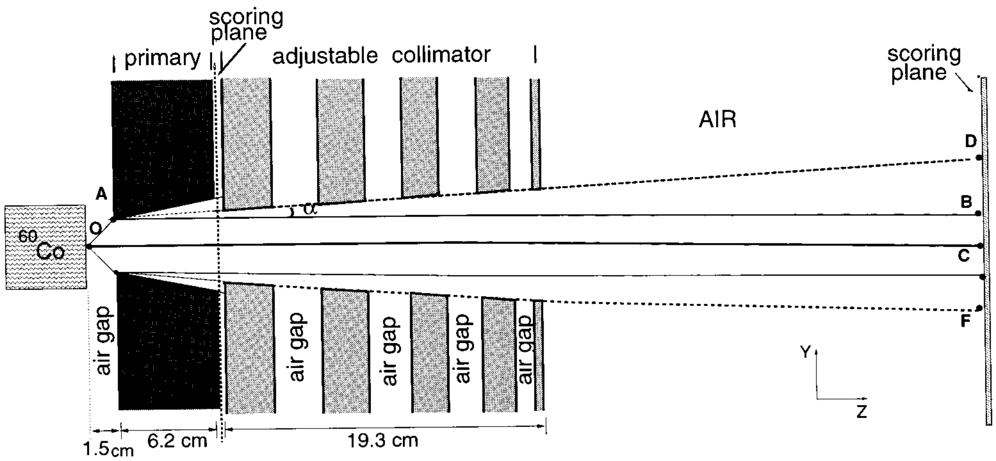

FIG. 1. The model of the Eldorado 6 ^{60}Co unit as used in the present study. The angle α changes with collimator opening and the faces are rotated to stay parallel to the edge of the field. Field size at the scoring plane is represented by DF. The realistic rectangular geometry of the collimator assembly about the beam axis (OC) is modeled. The complex leaf structure is simulated in detail for each field size. The one simplification in the model is that the leaves are not interlocked but surround the beam on the same layer. Different thicknesses of the air slab are simulated.

to give the correct overall mass of material. The surrounding heavy metal sleeve is modeled by an equivalent thickness in g/cm^{2}of Fe. A lead wall 2 cm thick (considered to be nearly equivalent to a thick wall) is included to simulate the source housing. The ^{60}Co radiates uniformly into 4π and the bare source has two equiprobable gamma rays at 1.17 and 1.33 MeV.

2. The collimation system

In modeling, we have used the realistic rectangular geometry of the collimator assembly. After the capsule there is a 1.5 cm air gap and then the fixed primary collimator (Fig. 1), which is made of solid heavymet alloy (90% W, 6% Ni, 4% Cu, ρ=16.9 g/cm^3) with a thickness of 6.2 cm. The primary collimator is followed by a 0.4 cm air gap and the outer collimator which extends over 19.3 cm.

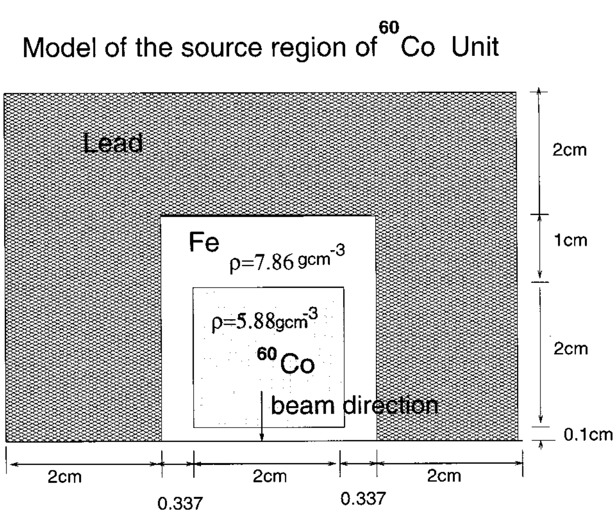

FIG. 2. The model used to simulate the source region including the radioactive material, the surrounded iron capsule and the lead shielding.

The outer collimator is movable and made of a series of lead leaves ''interlocked'' in the x and y directions. The one simplification in the model is that these are not interlocked but surround the beam on the same layer. The entire leaf collimator structure pivots about a hinge at the inner corner of the primary collimator (point A on Fig. 1). This way the face is always aligned with the field edge for the different field sizes (although it means other faces are not strictly perpendicular to the z-axis as they are in the model). The field size is defined by the straight line joining the points A and D. Since the field size (DF in Fig. 1) is symmetric about the central axis OC it can be expressed as DF=2 (DB+BC). Since the primary collimator does not move for different field sizes, BC is fixed at 1.4 cm. The primary collimator allows for an open field of 35×35 cm^2 at SSD=80.5 cm. The field size is given as DB+BC=tan(α)AB+BC=tan(α)(SSD −1.5)+1.4, where α is the angle between the lines AB and AD and it changes with the collimator opening.

We have modeled different leaf collimator openings to get field sizes from 5×5 to 35×35 cm^2 at a source-surface-distance (SSD) equal to 80.5 cm. The setting of each leaf of the adjustable collimator structure is modeled in detail for each field size.

B. Monte Carlo calculations techniques

In this section we describe the different stages of the simulation of the ''Eldorado 6,'' the principal features of the BEAM-EGS4[7] code we applied, the transport parameters of the simulation and the variance reduction techniques used.

1. The structure of the calculation

In the simulation of the full therapy unit we have split the calculation into three steps in order to save time.

In the first step, which takes the most computing time, 1.7×10^9 photons are initiated uniformly throughout the source material region and have an isotropic distribution.The primary collimator is also included in this step. The output of this step is a phase space file containing the energy, position, direction, charge and history variable for every particle exiting downstream from the primary collimator. The data for 60×10^6 particles reaching the scoring plane before the outer collimator are stored in a compressed format phase space file of 1.7 Gbytes.[7] Since the source and primary collimator do not move during the adjusting of the outer collimator for different openings, it is possible to use this phase space data for the simulation of all field sizes. Thus, this large set of particles is used repeatedly as the input to the next step of simulation.

The second step of the calculation simulates the passage of the particles through the adjustable leaf collimator and the air to the SSD plane. We simulate different openings of the outer collimator to get field sizes from 5×5 to $35\times 35\ \mathrm{cm}^2$ at an SSD equal to 80.5 cm. Different thicknesses of the air slab between the outer collimator and the patient plane are simulated (for calculations at SSD values of 72, 80.5, and 100 cm). We use the variable LATCH,[7] which allows us to store each particle's history during the first and the second step of the beam simulation. Therefore, we are able to determine if a particle is scattered in the source region, primary collimator, adjustable collimator or air slab before reaching the scoring plane. This information will be used in the next step to calculate the fluence and energy spectra of the particles scattered by different regions.

In the third step of the simulation, the phase space files for field sizes of 5×5 and $35\times 35\ \mathrm{cm}^2$ at an SSD of 72 cm are reused by the BEAM code as an input to the dose calculations in a water phantom. In both cases we transport the particles through a large phantom (40 cm diameter by 13 cm thick). The depth-dose curves in the buildup region are calculated for on-axis scoring regions 2 cm in radius and 0.025 cm thick and are presented in Sec. III F. Auxiliary calculations for 1 cm radius scoring regions for the 5×5 beam indicated that the depth-dose curve near the surface was not sensitive to the radius used.

The data analysis program BEAMDP[10] is used to analyze the phase space data files to extract the energy spectra of all particles reaching the plane at SSD=80.5 cm, and also the spectra of particles scattered from the source region or from collimators.

Statistical uncertainties are determined by breaking all calculations into ten batches and then computing the standard deviation on the mean values of the ten batches. However, this leads to an overestimate of the uncertainty in the relative output factor calculations because we use the same phase space file for the different settings of the jaw and thus the runs are highly correlated (see Sec. II C).

In the first step of the simulation (capsule and primary collimator), the global energy cutoffs for particle transport are set to ECUT=0.600 MeV and PCUT=0.010 MeV. However, we override the global ECUT with higher values of ECUT defined for individual regions in order to increase the efficiency of calculation (e.g., there is no electron transport in the source capsule except in the iron on the front face). The low energy thresholds for the production of knock-on electrons is set to AE=0.521 MeV (total energy) and the threshold for bremsstrahlung events is set to AP=0.010 MeV.

In the second step of the simulation (leaves and air gap to phantom) we use the same global energy cutoffs as in the first step. However, in the lead leaves and air inside the collimation system we override the global ECUT with the local value of 0.700 MeV. For these regions we use AE=0.700 MeV, while in the air between the collimation system and the SSD plane the value of AE is equal to 0.521 MeV. For the field sizes of 5×5 and $35\times 35\ \mathrm{cm}^2$ we use a lower global ECUT since the goal of these simulations is to create the input file to be used to calculate the depth-dose curves in the water phantom. Thus, to avoid underestimating the surface dose we transport the electrons to an ECUT value of 0.521 MeV.[3]

2. Range rejection of electrons

Although we break the simulation into three stages and reduce the time required for our calculation with the ''adequate'' choice of the transport parameters, the transport of all electrons originating in the complex geometry of the therapy unit to ECUT is a very time consuming task. Therefore we apply a variance reduction technique called ''range rejection of electrons.''[7,11,12] BEAM stops tracking an electron history if the particle cannot get out of the present region with enough energy to reach the scoring plane. This technique saves a significant amount of CPU time. In the first step, using range rejection in the capsule, housing and primary collimator increases the efficiency of calculation by a factor of 2. In the second step, using range rejection in the lead leaves and in the air slab reduces the time required for a calculation by a factor of 4.

C. Air-kerma calculations using realistic photon beam

This section presents the method we use to calculate the air-kerma output factors. The output factor is defined as the ratio of the output in air for a given field to that for a reference field.[13] Mathematically,

$$K_{\mathrm{output}}(i)=\left(\frac{K_i}{K_{\mathrm{ref},}}\right), \tag{1}$$

where the air-kerma value K_i for each field size i is given by

$$K_i=1.0032\int_0^{E_{\max}}\Psi_i(E)\left(\frac{\mu_{en}}{\rho}\right)dE, \tag{2}$$

where μ_{en}/ρ are mass energy- absorption coefficients, 1.0032 converts from collision kerma to total kerma[14] and $\Psi_i(E)$ is the central-axis photon energy fluence spectrum for a field size i given by

$$\Psi_i(E)=\Phi_i(E)E, \tag{3}$$

where $\Phi_i(E)$ is the energy spectrum of photon fluence for a field size i. These spectra have bin widths of 0.01 MeV, and are calculated at SSD=80.5 cm in a 2×2 cm^2 region about the beam axis. Mass energy-absorption coefficients for air are taken from Hubbell and Seltzer[15] with logarithmic interpolation of the tabulated coefficients. The uncertainty on the kerma is determined as the quadrature sum of the uncertainties coming from the calculated fluence spectrum only. Calculating the uncertainties on the relative output factors is more complex because we use the same phase space file after the fixed primary collimator for calculating the on-axis spectrum for each different field size. We have shown that the on-axis kerma from primaries is identical for all field sizes, and hence we can write

$$K_i = K_{\text{prim}} + K_i^{\text{scatt}}, \tag{4}$$

from which we see for the reference field size,

$$K_{\text{prim}} = K_{\text{ref}} - K_{\text{ref}}^{\text{scatt}}. \tag{5}$$

Therefore,

$$K_i = K_{\text{ref}} + K_i^{\text{scatt}} - K_{\text{ref}}^{\text{scatt}}, \tag{6}$$

and hence

$$K_{\text{output}}(i) = 1 + \frac{K_i^{\text{scatt}} - K_{\text{ref}}^{\text{scatt}}}{K_{\text{ref}}}. \tag{7}$$

As will be seen below, the scattered components contribute no more than 30% of the air kerma and the second term on the right-hand side is less than 0.1. Thus the overall uncertainty on $K_{\text{output}}(i)$ is much smaller when calculated from Eq. (7) than from Eq. (1) because the common uncertainty on K_{prim} is removed.

III. RESULTS

A. The effects of the source capsule

Only 28 particles reach the front face of the capsule for every 100 photons from ^{60}Co decay. At the front face of the capsule most particles are photons, and electrons represent only 0.5% of the particles. These electrons have an average energy of 616 keV. Scattered photons represent 28% of the photon fluence at the front face of the capsule.

B. Comparison of on-axis spectrum with previously published spectrum

Figure 3 shows the on-axis photon spectrum calculated in the present BEAM simulation for a broad beam (35×35 cm^2) at 100 cm SSD, and compares the spectrum to the previous EGS4 published spectrum.[3] The present values of the fluence for primary photons agree with those calculated previously to within 1.5% for energies of 1.17 MeV and 3.7% for 1.335 MeV. However, there are discrepancies in the scattered photon parts of the spectra. The present results are between 2% and 34% higher than in the previous calculations although the shapes are reasonably similar. As seen below in Fig. 9, there is a significant number of photons scattered from the

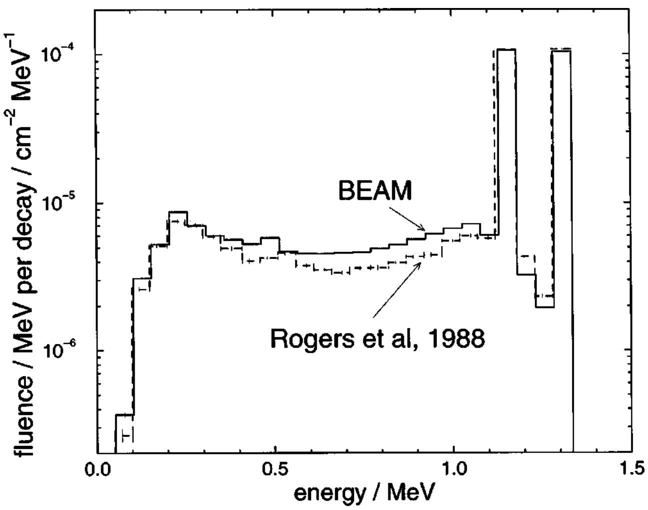

FIG. 3. The calculated on-axis photon spectrum at 100 cm SSD for a 35×35 cm^2 field size is compared with a previously published spectrum (Ref. 3) also calculated with EGS4. The additional scatter in the current calculations is at least partially accounted for by the inclusion of the lead shield around the capsule and the detailed modeling of the collimator.

lead shield around the source capsule and this was not modeled previously.[3] This would explain most of the difference up to about 700 keV photon energy. Similarly, we show below that modeling the adjustable collimator as leaves, instead of as solid collimator, increases the scatter from the collimator and we show that the spectrum of photons from the collimator are mostly above 700 keV. Thus this improvement in the present model would likely explain the difference in this portion of the spectrum.

C. Field size effects on spectra

In this section we present the on-axis fluence and energy spectra of the particles at SSD of 80.5 cm for different field sizes and study the contributions of the different scattered components to the spectra.

1. On-axis photon and electron spectra at SSD versus field size

Figure 4 shows the relative fluence of the photons and the different components of the fluence reaching the plane at SSD=80.5 cm vs field size. All values are normalized to the total photon fluence calculated for a 30×30 cm^2 field size. The number of primaries and the number of photons scattered only by the source region remain relatively constant as the field size increases, and represent 62% and 28% of the total number of photons. The photons from the source region include a component from the lead shield surrounding the source capsule which is a constant 2.5% except for the field sizes less than 10×10 cm^2. The total number of photons increases about 10% from 7×7 to 30×30 cm^2 field size. Figure 4 also shows the increase with field size of the fluence of photons scattered from the primary and adjustable collimator. For a field size of 7×7 cm^2, the number of photons scattered from the collimation system represents less than

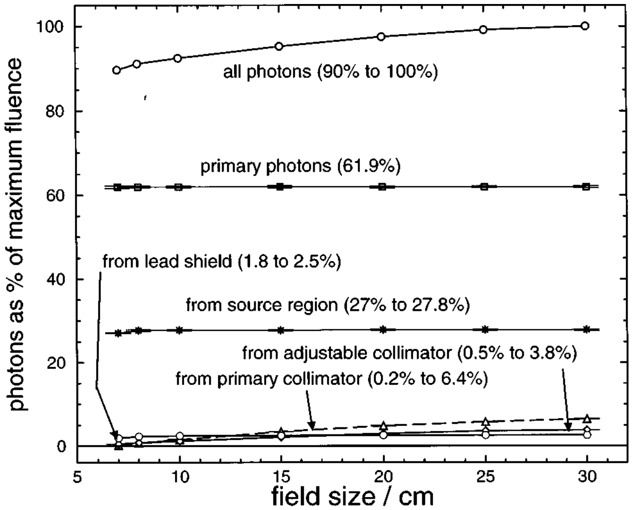

FIG. 4. Photon fluence versus field size of various components reaching a plane at SSD=80.5 cm. The number of photons is normalized to the total photon fluence for the maximum field size (30×30 cm^2). The fluence is scored in a 2×2 cm^2 region on the axis.

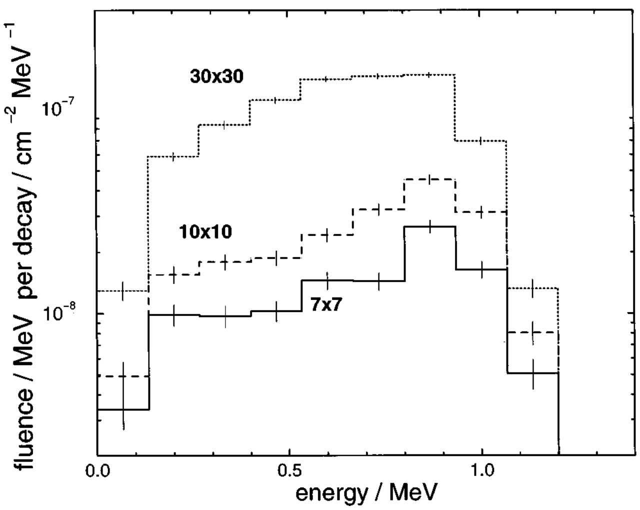

FIG. 6. The on-axis energy spectrum of electrons reaching the scoring plane at 80.5 cm SSD for three different field sizes (7×7, 10×10 and 30×30 cm^2). The spectra are calculated for scoring regions of 8×8 cm^2 (results are similar for a 6×6 cm^2 scoring region for the small field because the electrons spread well outside the photon beam).

1% of the total number reaching 80.5 cm SSD, while for a field size of 30×30 cm^2 the contribution is equal to 10%, about 6.4% from the primary and 3.8% from the adjustable collimator. This scatter explains the observed variation of the total number of photons with field size and is qualitatively consistent with the results of Han *et al.*[4]

The on-axis photon energy spectra shown in Fig. 5 are calculated in a 2×2 cm^2 region. The figure compares the photon spectra for three different field sizes. The fluence of photons is not significantly different for the three cases below the 511 keV peak, but at higher energies the scattered photon fluence increases significantly with field size. For energies about 1 MeV the collimator effect is clearly evident in the spectra (especially for a 30×30 cm^2 field). Figure 5 also shows the percentage of the photon fluence from scattered photons. The corresponding values in terms of energy fluence are 17%, 19%, and 24%, respectively, for the 7×7, 10×10 and 30×30 cm^{2}field sizes. The percentage of the air kerma or dose from scattered photons is related more closely to the percentage of energy fluence because the mass energy absorption coefficients are nearly constant in this energy region.

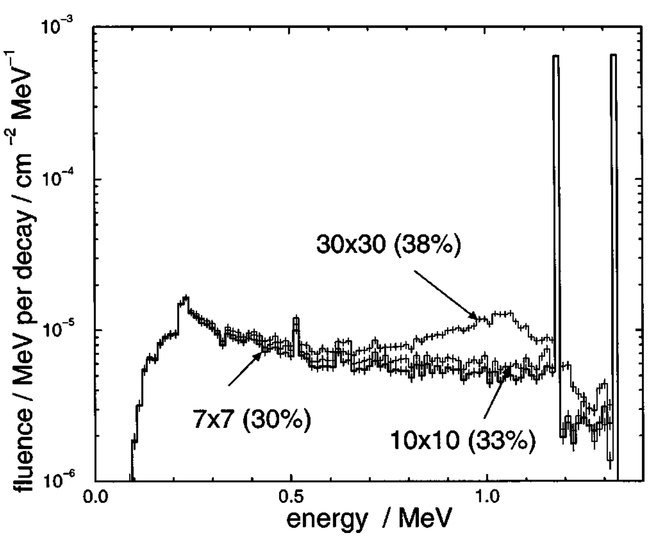

FIG. 5. On-axis energy spectra of photons reaching the scoring plane at 80.5 cm SSD for three different field sizes (7×7, 10×10 and 30×30 cm^2). The spectra are calculated for scoring regions of 2×2 cm^2. Energy bins are 10 keV wide. The percentage of the total fluence from scattered photons is shown in brackets. The corresponding values in terms of energy fluence are 17%, 19% and 24%, respectively, for the 7×7, 10×10 and 30×30 cm^2 field sizes.

The electron spectra shown in Fig. 6 are calculated for a larger region (8×8 cm^{2}instead of 2×2 cm^{2}in the photon case) because of the poorer statistics. We see that the electron fluence is about seven times bigger for a 30×30 cm^2 beam than for a 7×7 cm^2 beam. The average energy of electrons is about 600 keV. Although the electron fluence is a factor of about 100 less than the photon fluence even for the largest field, it must be remembered that the dose delivered per unit fluence of electrons is typically 100 times greater than for photons.[16]

Figure 7 presents the variation in electron fluence as a function of field size. The electron contamination increases overall by a factor of about seven from the smallest to the largest fields shown. The largest source of electrons is the capsule itself for small field sizes, but for the larger field sizes the collimator system becomes a larger source of electron contamination.

2. Spectra of scattered photons for different field sizes

Figures 8 and 9 present the scattered photon energy spectra for a small and large field size. Several scattered photon

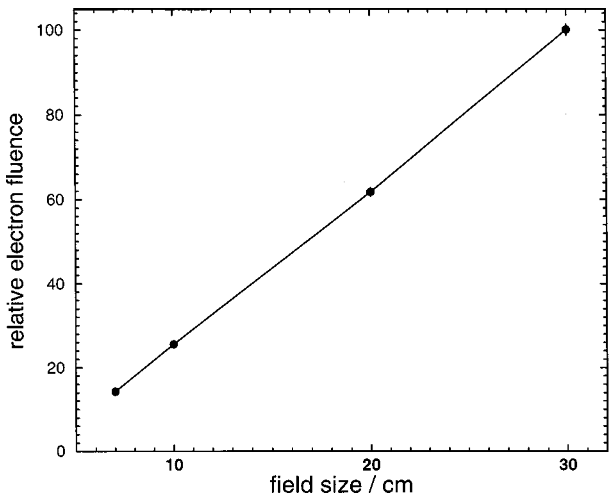

FIG. 7. Variation in electron contamination with field size for an 8×8 cm^2 area on the central axis at an SSD of 80.5 cm.

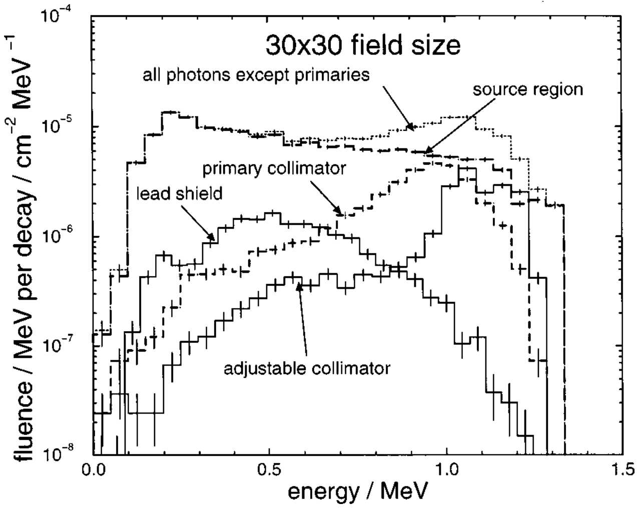

FIG. 9. The on-axis energy spectrum of all scattered photons reaching the scoring plane at 80.5 cm SSD for a 30×30 cm^2 field size. The spectra of photons scattered from different parts of the ^{60}Co unit are also shown.

components of the energy spectra are also shown. For the 7×7 cm^2 field size, the source region component is practically equal to the total spectrum of scattered photons, but for the 30×30 cm^2 field size the contribution from the collimation system increases with energy, and in the region of about 1 MeV is practically equal to the number of photons originating in the source region. The contribution from the primary collimator is higher than from the adjustable collimator until the peak about 1 MeV. After that, the number of photons scattered from the adjustable collimator is higher. This is because photons from the adjustable collimator are usually more forward scattered and hence higher in energy. Figure 9 shows the contribution from the lead shield about the capsule. It is roughly the same for other field sizes and contributes about 10% of the scatter contribution from the source region.

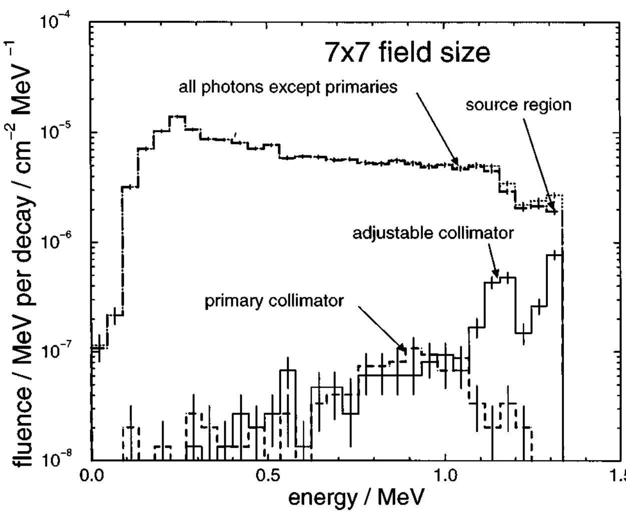

FIG. 8. The on-axis energy spectrum of all scattered photons reaching the scoring plane at 80.5 cm SSD for a 7×7 cm^2 field size. The spectra of photons scattered from different parts of the ^{60}Co unit are also shown.

D. Air-kerma output factors

1. Comparison of calculated and measurement beam output factor

Using Eq. (7), we calculate the kerma output factors for field sizes from 7×7 to 30×30 cm^2 relative to the reference field of 8×8 cm^2. The calculated output factors, with a relative uncertainty of 0.2%, are compared to the measured values in Fig. 10. The 10% variation in output factor is clearly observed and reproduced by the calculations. The calculated values agree with the measurements to within 0.1%. Measured data are from Ken Shortt and Dave Hoffman from NRCC. These results are quantitatively different from the

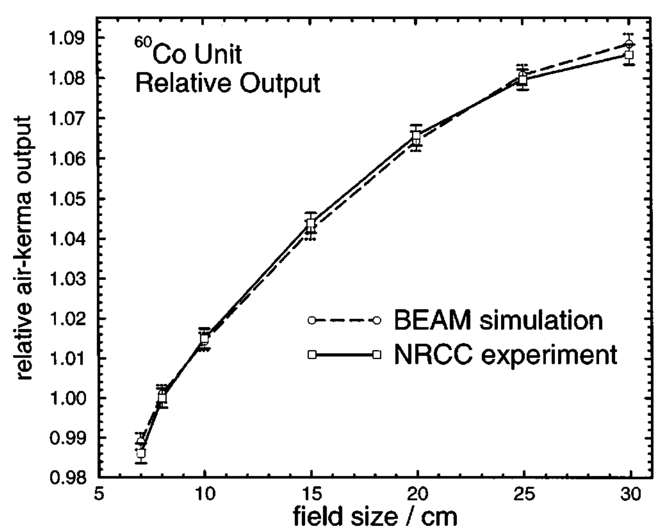

FIG. 10. Comparison of calculated and measured relative air-kerma output factors vs field size for Eldorado 6 ^{60}Co unit at NRC. Experimental data are normalized relative to the 8×8 cm^2 field. The values of kerma are determined for the on-axis region of 2×2 cm^2. The calculated data are normalized to give the best overall fit to the measured data (i.e., no special status is given to the calculated value for the 8×8 cm^2 field).

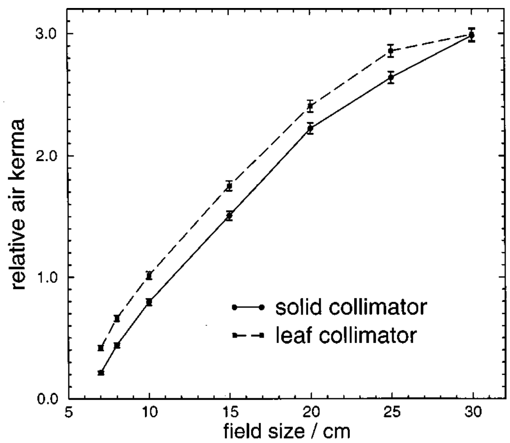

FIG. 11. Air-kerma values at SSD=80.5 cm from photons scattered in the adjustable collimator calculated using detailed modeling of the leaf collimator or calculated using a simplified model of solid rectangular leaves. The values of kerma are determined for the central-on-axis (2×2 cm^2).

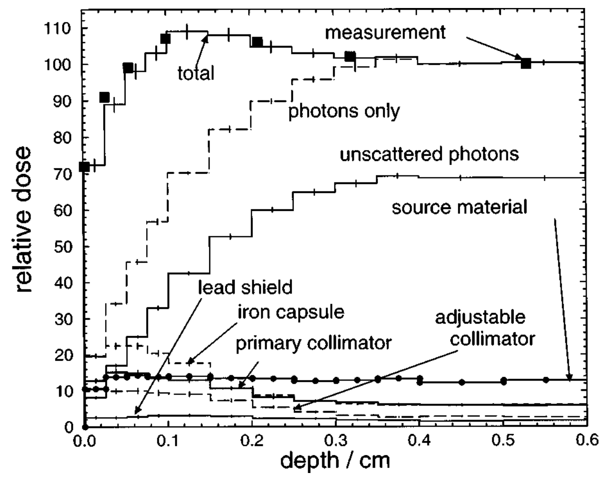

FIG. 12. Comparison of the measured (Ref. 9) and calculated central-axis buildup dose curve at an SSD of 72 cm for field size of 35×35 cm^2 (defined at SSD=80.5 cm). The components of the dose, which are scattered from various parts of the head, are also shown with the photon component of the dose. The curves are normalized to 100% for 0.45 cm depth.

results of Han *et al.*, who measured a variation of 6.9% for 35×35 cm^2 field size compared to a 10×10 cm^2 field size (which is roughly consistent with our measured values) while they calculated a variation of 14%.[4]

E. Effects of the collimator geometry

In this section we study the influence of the leaf structure of the collimation system in the collimator scattering. For this purpose, calculations of the air-kerma values are done using two different geometries: (i) proper modeling of the leaf collimator (see Fig. 1) and (ii) an approximation using solid leaves.

We calculate the central on-axis energy spectra of the photons scattered by the outer collimator and reaching the scoring plane for both geometries. The collimator opening in the two cases is modeled to get a field size of 10×10 cm^2 at 80.5 cm and the photons are scored in a region of 2×2 cm^2 about the beam axis.

The results of the simulation indicate an increase of photon fluence for energies greater than 700 keV for the case of the leaf collimator relative to the solid collimator. Since the thickness of the leaves is between 2 and 3 cm, some photons which couldn't escape from the solid collimators (19.3 cm thick) can escape from the leaves and reach the scoring plane.

Next we calculate the air-kerma values from collimator scattered photons for the two cases using the methods of Sec. II C. Figure 11 compares the air-kerma values versus field size for both geometries. There is a difference of about 3% between the two curves, and they have approximately the same shape. However, since the total contribution is only 4% from these scattered photons (see Fig. 4), the effect on the overall kerma is negligible.

F. Depth-dose curves

In this section we investigate the influence of electron contamination in a broad (35×35 cm^2) and a narrow (5×5 cm^2) ^{60}Co beam on the dose buildup curves in a homogeneous water phantom.

Figures 12 and 13 compare the measured relative central-axis depth-dose curves for broad and narrow beams[9] with the calculated total dose curve and the calculated components of the dose due only to the photons. These curves are normalized to the dose at the depth of dose maximum in the absence of electron contamination (0.45 cm). The effects of the electron contamination on the dose buildup curve are clearly seen from the difference between the total and the photon dose in the first 3.5 mm from the surface for both field sizes. For the field size of 35×35 cm^2 the contaminant electrons are responsible for the increase of the relative surface dose from about 19% to 72%. At the same time, the dose maxi-

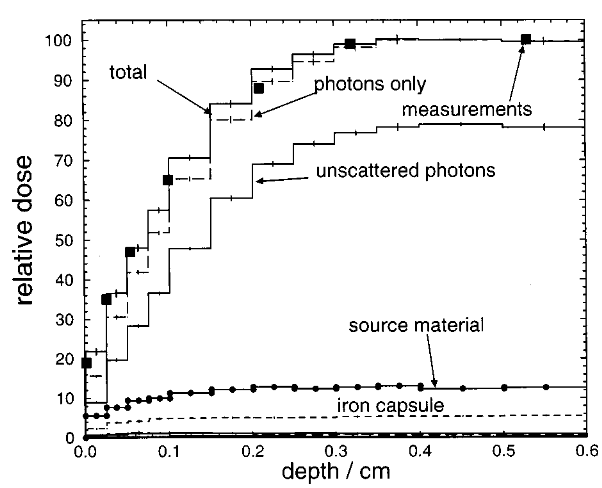

FIG. 13. Same as for Fig. 12, but for the narrow beam of ^{60}Co (field size of 5×5 cm^2).

mum increases by 9% and moves from 5 to 1.2 mm. For a 5×5 cm^2 field the influence of electron contamination is not so significant; the increase on the relative surface dose is only about 6% and has no effect on the location of dose maximum.

The agreement between calculated and measured[9] central-axis depth-dose curves is excellent. This agreement is much better than reported for the previous calculations for a broad beam,[3] especially at the surface where the previous work only calculated a relative dose of 40%. The previous calculations contained many approximations which the authors recognized affected the surface dose calculation in particular.[3] These approximations are not needed using the BEAM code.

Figures 12 and 13 also show the dose components for particles scattered from different parts of the ^{60}Co unit. In the narrow beam only the source material and source capsule container play any role at all, with the primaries representing about 80% of the photon dose at most depths. In the broad beam the primaries contribute only about 70% of the total photon dose at depth. Near the surface the contribution from electrons from the iron capsule is evident and that from both the collimators becomes important near the surface. For the broad beam there is a small component of the dose from photons scattered by the lead shield about the source capsule.

IV. CONCLUSIONS

The 10% variation of air-kerma output with field size is due almost entirely to increased collimator scatter and not related to the shadowing of primary photons as would happen in accelerators. There is a minor shadowing of the scatter from the lead shield around the capsule. Detailed modeling of the collimator leaves, instead of a simplified model, increases the contribution from the leaves by 3%. This has little effect on the overall output variation and does not explain the difference between our results and those of Han *et al.*,[4] who did not correctly predict the variation in output with field size. For a broad beam (35×35 cm^2), the electron contamination increases the relative surface dose from 19% to 72% and moves the dose maximum from 5 to 1.2 mm. However, for a 5×5 cm^2 field size the increase on the relative surface dose due to electrons is only about 6%. The BEAM code can be said to model the ^{60}Co unit accurately since it properly predicts both the variation in output factors with field size and also the dramatic variation in depth-dose curves with field size.

ACKNOWLEDGMENTS

We would like to thank Ken Short and Dave Hoffman for providing us with the measured air-kerma outputs vs field size, and David Marchington for help measuring the source dimensions. We wish to thank Daryoush Sheikh-Bagheri and Blake Walters for many discussions about the BEAM code, and Jan Seuntjens for providing some very useful routines.

APPENDIX: ON-AXIS PHOTON SPECTRA FOR 10×10 AND 35×35 cm^2 FIELD SIZES AT 100 SSD

TABLE I. On-axis photon spectrum from an Eldorado 6 ^{60}Co unit for 35×35 and 10×10 cm^2 field sizes at SSD=100 cm. They are calculated including capsule, collimator and air scatter. The values are normalized per decay in the source capsule. One standard deviation uncertainties are given in brackets.

Top of bin/MeV	Photon fluence/MeV per decay/cm^{-2} MeV^{-1} 10×10	35×35
0.05	6.600e-08 (30%)	8.400e-08 (26%)
0.10	3.360e-07 (13%)	3.660e-07 (10%)
0.15	3.324e-06 (4%)	3.366e-06 (4%)
0.20	5.670e-06 (3%)	5.748e-06 (3%)
0.25	8.778e-06 (3%)	9.006e-06 (2%)
0.30	7.410e-06 (3%)	7.674e-06 (3%)
0.35	5.952e-06 (3%)	6.204e-06 (3%)
0.40	5.640e-06 (3%)	6.066e-06 (3%)
0.45	5.118e-06 (3%)	5.772e-06 (3%)
0.50	5.784e-06 (3%)	6.510e-06 (3%)
0.55	4.140e-06 (4%)	4.704e-06 (3%)
0.60	4.002e-06 (4%)	4.752e-06 (3%)
0.65	4.338e-06 (4%)	5.166e-06 (3%)
0.70	3.804e-06 (4%)	4.818e-06 (3%)
0.75	3.834e-06 (4%)	5.076e-06 (3%)
0.80	3.768e-06 (4%)	5.022e-06 (3%)
0.85	3.672e-06 (4%)	5.538e-06 (3%)
0.90	3.852e-06 (4%)	6.258e-06 (3%)
0.95	3.600e-06 (4%)	6.822e-06 (3%)
1.00	3.684e-06 (4%)	7.350e-06 (3%)
1.05	3.168e-06 (4%)	7.908e-06 (3%)
1.10	3.696e-06 (4%)	6.684e-06 (3%)
1.175	1.128e-04(0.7%)	1.114e-04(0.7%)
1.20	1.434e-06 (6%)	3.570e-04 (4%)
1.25	1.860e-06 (5%)	2.208e-06 (5%)
1.335	1.131e-04(0.7%)	1.125e-06(0.7%)

[a]Electronic mail: dave@irs.phy.nrc.ca

1 J. H. Aitken and W. H. Henry, ''Spectra of the internally scattered radiation from large ^{60}Co sources used in teletherapy,'' Int. J. Appl. Radiat. Isot. **15**, 713–724 (1964).
2 ICRU, ''Specification of high-activity gamma-ray sources,'' ICRU Report 18, ICRU, Washington, D.C., 1971.
3 D. W. O. Rogers, G. M. Ewart, A. F. Bielajew, and G. van Dyk, ''Calculation of electron contamination in a ^{60}Co therapy beam,'' in *Proceedings of the IAEA International Symposium on Dosimetry in Radiotherapy* (IAEA, Vienna, 1988), Vol. 1, pp. 303–312.
4 K. Han, D. Ballon, C. Chui, and R. Mohan, ''Monte Carlo simulation of a cobalt-60 beam,'' Med. Phys. **14**, 414–419 (1987).
5 D. R. Shipley and S. Duane, ''Determination of photon fluence spectra from the NPL Mobaltron ^{60}Co Unit,'' Technical Report RSA (EXT) 46, NPL, Teddington, UK, 1994.
6 F. M. Khan, W. Sewchand, J. Lee, and J. F. Williamson, ''Revision of tissue-maximum ratio and scatter-maximum ratio concepts for cobalt-60 and higher energy x-ray beams,'' Med. Phys. **7**, 230–237 (1980).
7 D. W. O. Rogers, B. A. Faddegon, G. X. Ding, C. M. Ma, J. Wei, and T. R. Mackie, ''BEAM: A Monte Carlo code to simulate radiotherapy treatment units,'' Med. Phys. **22**, 503–524 (1995).
8 W. R. Nelson, H. Hirayama, and D. W. O. Rogers, ''The EGS4 Code System,'' Report SLAC-265, Stanford Linear Accelerator Center, Stanford, California, 1985.
9 F. H. Attix, F. Lopez, S. Owolabi, and B. R. Paliwal, ''Electron contamination in ^{60}Co gamma-ray beams,'' Med. Phys. **10**, 301–306 (1983).

[10] C. M. Ma and D. W. O. Rogers, ''BEAMDP as a general-purpose utility,'' NRC Report PIRS 509e, 1995.
[11] A. F. Bielajew and D. W. O. Rogers, ''Variance-reduction techniques,'' in *Monte Carlo Transport of Electrons and Photons*, edited by T. M. Jenkins, W. R. Nelson, A. Rindi, A. E. Nahum, and D. W. O. Rogers (Plenum, New York, 1989), pp. 407–419.
[12] A. F. Bielajew and D. W. O. Rogers, ''Variance reduction techniques,'' National Research Council of Canada Report PIRS-0396, 1993.
[13] F. M. Khan, *The Physics of Radiation Therapy* (Williams and Wilkins, Baltimore, Maryland, 1984).
[14] D. W. O. Rogers, ''Fundamentals of high energy x-ray and electron dosimetry protocols,'' in *Advances in Radiation Oncology Physics, Medical Physics Monograph 19*, edited by J. Purdy (AAPM, New York, 1992), pp. 181–223.
[15] J. H. Hubbell and S. M. Seltzer, ''Tables of x-ray mass attenuation coefficients and mass energy-absorption coefficients 1 keV to 20 MeV for elements $Z=1$ to 92 and 48 additional substances of dosimetric interest,'' Technical Report NISTIR 5632, NIST, Gaithersburg, MD 20899, 1995.
[16] D. W. O. Rogers, ''Fluence to dose equivalent conversion factors calculated with EGS3 for electrons from 100 keV to 20 GeV and photons from 20 keV to 20 GeV,'' Health Phys. **46**, 891–914 (1984).